Optics Letters

Optical topography of rough surfaces using vortex localization of fluorescent markers

PETR SCHOVÁNEK,[1,2] PETR BOUCHAL,[3,4,*] AND ZDENĚK BOUCHAL[1]

[1]Department of Optics, Palacký University, 17. listopadu 1192/12, 771 46 Olomouc, Czech Republic
[2]Meopta-optika, s.r.o., Kabelíkova1, 750 02 Přerov, Czech Republic
[3]Institute of Physical Engineering, Faculty of Mechanical Engineering, Brno University of Technology, Technická 2, 616 69 Brno, Czech Republic
[4]Central European Institute of Technology, Brno University of Technology, Purkyňova 656/123, 612 00 Brno, Czech Republic
*Corresponding author: petr.bouchal@ceitec.vutbr.cz

Received 5 March 2020; revised 13 June 2020; accepted 1 July 2020; posted 6 July 2020 (Doc. ID 392072); published 7 August 2020

Measuring rough surfaces is challenging because the proven topographic methods are impaired by the adverse effects of diffuse light. In our method, the measured surface is marked by fluorescent nanobeads allowing a complete suppression of diffuse light by bandpass filtering. Light emitted by each fluorescent bead is shaped to a double-helix point spread function used for three-dimensional bead localization on the surface. This non-interferometric measurement of rough surface topography is implemented in a vibration resistant setup. The comparison of our method with vertical scanning interferometry shows that a commercial profiler is surpassed when ground glass surfaces with steep slopes are measured.

https://doi.org/10.1364/OL.392072

Optical topography includes a wide range of techniques excellent in fast, accurate, non-contact and non-destructive mapping of smooth surfaces. These techniques are based on a variety of approaches including confocal microscopy [1], intentional introduction of chromatic aberration [2], fringe projection [3], focus variation microscopy [4], point autofocusing [5], and interferometry. To achieve high measurement accuracy, interferometric methods are becoming the preferred choice. In these methods, the surface topography is restored from optical path difference (OPD) introduced between signal and reference beams reflected from the measured sample and a high-quality reference surface, respectively. The measurement differs depending on the spectral and coherence properties of light. When quasi-monochromatic light is used, the measurement is typically based on phase-shifting interferometry [6] providing wide field topographic data from recordings taken repeatedly with a different phase shift [7]. The OPD exceeding the wavelength can still be measured by applying the phase unwrapping in the postprocessing of measured data [8] or by deploying multiwavelength interferometry [9]. The phase ambiguity problem can be effectively solved in techniques using white light with a short coherence length. In this case, the interference fringes are created only when optical paths of signal and reference beams are precisely matched. By the controlled vertical scanning of the sample and tracking the fringe corresponding to the zero OPD, the surface topography can be precisely restored [10]. Although the phase-shifting interferometry and the vertical scanning interferometry (VSI) are rather complementary in use, both techniques were combined to retain the high accuracy of the phase-shifting method free from the phase ambiguity problem [11].

The optical topography of smooth surfaces is well established in both science and technology, but its performance and usability are significantly reduced when the measured surface is rough. Assessing whether the surface is optically rough depends not only on the roughness, but also on the wavelength of light and the size of the diffraction spot of the imaging system used; the surface is optically rough when height variations in the diffraction spot exceed a quarter of the wavelength [12,13]. In the rough surface measurement, the VSI has become a commercially available technique, but its use still has some limitations. Theoretical considerations and experimental results showed that diffuse light prevents measurement of the true shape and that the measurement uncertainty increases with surface roughness [12,13]. Hence, the success of the rough surface topography depends on the capability to eliminate the adverse effects of diffuse light.

Here, we report on the optical topographic measurement of rough surfaces based on the vortex localization of fluorescent markers. We use fluorescent beads that are adherent to the measured surface and allow suppression of diffuse light by bandpass filtering. Information on the three-dimensional (3D) position of individual beads is obtained from fluorescent light; hence, the measurement is independent of the surface roughness. The developed method is inspired by the 3D super-resolution localization imaging that revolutionized fluorescence microscopy by single molecule imaging [14]. In advanced methods of localization microscopy [15,16] and particle tracking velocimetry [17], the depth of emitters is restored from the diffracted rotation of a specially engineered double-helix point spread function (DH PSF). To maximize the dynamic range of the topographic measurement, we deployed the DH PSF created by non-diffracting vortex beams. This DH PSF previously succeeded in the structured illumination topography of smooth surfaces [18] and the localization of dielectric, metal, and fluorescent nanoparticles in the axial range significantly exceeding the depth of focus [19].

Experiments were realized in the setup shown in Fig. 1(a). As measured samples, we used spherical surfaces with the same radius $R = 5$ mm but different roughness. The measured surfaces were marked by fluorescent polystyrene nanospheres (Phosphorex 2103 A) with average diameter $d = 500$ nm and peak excitation and emission wavelength 460 nm and 500 nm, respectively. Fluorescent nanospheres were stirred in a water solution and then applied on the measured surface. Individual nanospheres were randomly distributed over the surface during its drying thanks to Brownian motion [see Fig. 1(b)]. The prepared samples were placed in the object space of the microscope objective (MO) (20×, NA = 0.5, $f = 10$ mm) and illuminated using the mercury arc lamp, lenses IL1 and IL2 providing Köhler illumination, and the filter cube for green fluorescent protein (excitation filter EXF 469±18 nm, dichroic mirror DM, 452–490 nm/505–800 nm, emission filter EMF, 525±20 nm). Thanks to the fluorescence cube, the backscattered diffuse light is canceled, and only fluorescence emission contributes to the final image. Light emitted from nanospheres is collected by the MO and directed towards the first tube lens TL1 with the focal length $f = 200$ mm. The image created in the back focal plane of TL1 is Fourier transformed by the lens FL with the same focal length. Using 4 F system formed by TL1 and FL, the back focal plane of the MO is imaged to the plane, where the spiral mask (SM) is placed. The SM made by electron lithography is composed of two transparent annular areas (medium radii $R1 = 2.69$ mm, $R2 = 3.8$ mm, width $\Delta R = 0.25$ mm), in which the vortex phase with the topological charge +1 and −1 is imposed on the light leaving the inner and outer zones, respectively [Fig. 1(a)]. The second tube lens TL2 with the focal length $f = 400$ mm performs the Fourier transform of the light transmitted through the SM, which results in the generation of two non-diffracting Bessel beams with the opposite pitch of the helical wavefront. By the interference of these beams, the DH PSF is created, whose angular rotation determines the axial position of the emitting fluorescent bead. In measurement, the DH PSF arises for each fluorescent bead whose light is captured by the MO and transformed by the SM. In this way, an array of angularly rotated DH PSFs is created, mapping the surface depth at positions given by fluorescent beads. Each DH PSF is generated by the self-interference of two vortex beams originating from the same fluorescent bead, provided that the OPD does not exceed the coherence length. Light fields emitted by different fluorescent beads are not mutually correlated. The resulting image, formed by the intensity superposition of individual DH PSFs, is recorded by a CCD (XIMEA MR4021MC-BH, 2048 × 2048, pixel size 7.4 μm).

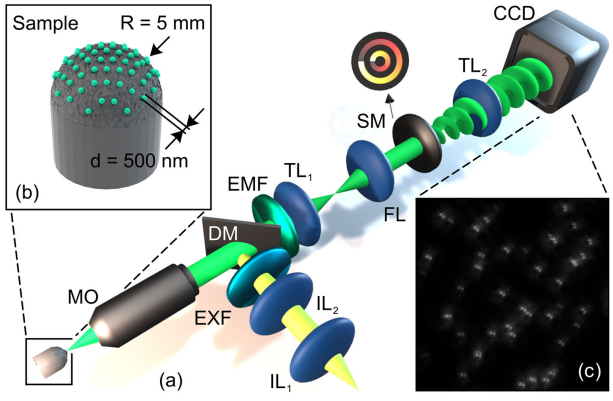

Fig. 1. Topography of rough surfaces using vortex localization of fluorescent markers. (a) Experimental setup: IL1, IL2, illumination lenses; EXF, excitation filter; DM, dichroic mirror; EMF, emission filter; MO, microscope objective; TL1, TL2, tube lenses; FL, Fourier lens; SM, spiral mask; and CCD, charge-coupled device. (b) Fluorescent nanospheres adherent to measured surface. (c) Measured DH PSFs with depth-induced angular rotation.

The rotation of the DH PSF becomes more sensitive to defocusing when the numerical aperture of the MO and the radii of annular zones in the SM are increased. This change in parameters adversely affects the axial measuring range, which is reduced. Higher rotation sensitivity can also be achieved by increasing the magnification of the imaging path. This results in a shortening of the axial measuring range and a reduced field of view due to the limited size of the CCD [18,19]. Hence, the system is designed to find a trade-off between accuracy, axial measuring range, and field of view. The parameters of our setup were chosen adopting the theoretical model in Refs. [18,19]. The system allows the measurement with a rotation rate 12 deg/μm, an axial range $\Delta z = 16$ μm, and a field of view 380 × 380 μm^2 (limited by CCD area) when evaluated in the object space. The developed system is built as a measuring probe whose field of view can be expanded by scanning. Here, the stitching of multiple images is done to demonstrate this possibility. The entire field of view comprises five sub-records taken by the gradual displacement of the sample.

In the developed method, the depth information is encoded in the angular rotation of the DH PSF. The surface topography is retrieved from a single shot by evaluating the angular orientation of DH PSFs, whose transverse coordinates correspond to the positions of fluorescent markers distributed on the surface [see Fig. 1(c)]. The 3D position of individual DH PSFs is determined using custom software prepared by Mathematica.

Workflow used in data processing is schematically illustrated in Fig. 2. In the first step, the contrast of raw images is enhanced by applying a deconvolution-based image processing algorithm. Subsequently, the measured DH PSFs are separated from the background by image segmentation. Problems with uneven fluorescence signal are overcome using an adaptive thresholding allowing the creation of binary images of DH PSFs [Fig. 2(a)]. In the next step, automated side lobe detection is applied to

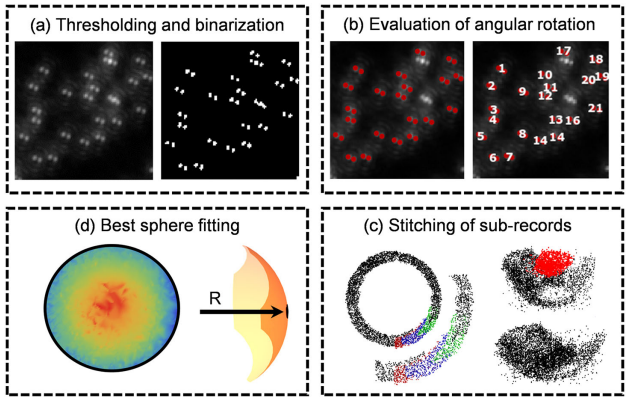

Fig. 2. Procedures of automated data processing used in measuring rough surface topography. (a) Deconvolution based adaptive data binarization. (b) Automated side lobe detection and determination of angular orientation of DH PSFs. (c) Stitching of sub-records (color-coded) and removing rotation ambiguity by data unwrapping. (d) Surface reconstruction and best sphere fitting.

binary DH PSFs. The side lobes of each DH PSF are paired, and their centers of gravity calculated. The vectors connecting the centroids are used to determine the angular orientation of individual DH PSFs. The transverse coordinates of the center of gravity, calculated for DH PSF consisting of both lobes, are assigned to its angular rotation to obtain depth information at given lateral positions [Fig. 2(b)]. Lateral positions of fluorescent markers in the object space are calculated using the magnification of the imaging system. The procedure is repeated for all sub-records [color-coding in Fig. 2(c)] taken by a sequential displacement of the sample. Image areas forming the enlarged field of view are stitched with a slight overlapping at boundary regions. The ambiguity in angular rotation (angles exceeding 180°), occurring in stitched images, is solved using procedures based on the phase unwrapping [8] [Fig. 2(c)]. The surface topography is obtained from the dependence of the angular rotation $\Delta\Phi$ of DH PSF on the defocusing Δz (axial position of fluorescent nanosphere). According to theory, this dependence is linear with the slope determined by the basic parameters of the optical system. Because these parameters are known with limited accuracy, the dependence of $\Delta\Phi$ on the Δz must be obtained by calibration measurement. The measurement results in the mapping of the surface by a cloud of points for which the depth is determined in the lateral positions determined by fluorescent markers. In the final operation, the best sphere fitting of the measured spherical surface is done [Fig. 2(d)].

The calibration measurement was performed with a fluorescent nanosphere whose axial position was precisely varied with 1 μm step over a range of 10 μm using an interferometrically calibrated piezoelectric transducer. During z-stacking, DH PSFs were recorded and their angular rotations $\Delta\Phi$ evaluated as a function of the axial displacement Δz. Results of the calibration measurement are illustrated in Fig. 3(a), where circles and error bars represent the mean value and the standard deviation 3σ of 20 independent measurements, respectively. The slope of the straight line obtained by the linear regression was used in all rough surface measurements for angle to depth conversion. The rotation rate $\Delta\Phi/\Delta z = 12.13$ deg/μm, obtained experimentally, is in good agreement with the theoretical value 12.35 deg/μm [18]. The accuracy of the measurement can be assessed according to Fig. 3(b), where circles represent the deviation of the mean value of measured depths from the depths given by the calibration regression line in Fig. 3(a). The results show that the accuracy of the measurement remains better than 0.5 μm in the axial range of 16 μm.

The developed method was tested by measuring the topography of spherical surfaces made of N-BK7 glass. The samples were prepared using diamond grinding tools with different

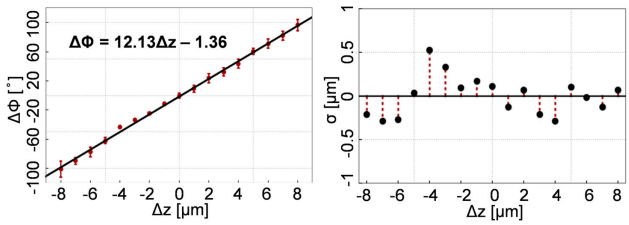

Fig. 3. Results of calibration measurement. (a) Dependence of angular rotation $\Delta\Phi$ of DH PSF on ground truth depth Δz. (b) Deviation of the mean value of measured depths σ from the depth obtained using regression line in (a).

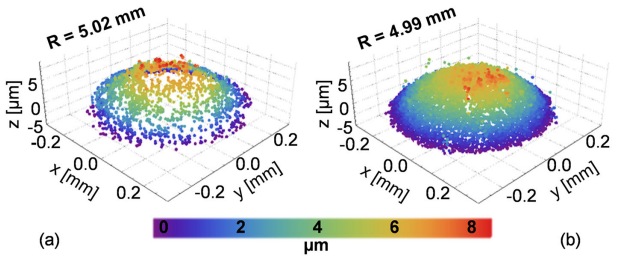

Fig. 4. Topography of a spherical surface with the nominal production radius $R = 5$ mm and the mean roughness $R_a = 0.85$ μm measured by (a) vortex localization technique and (b) commercial 3D profiler.

grit size (D15, D46 and D64) and provided by the company Meopta-optika, s.r.o. All surfaces have the same nominal production radius R = 5 mm but different roughness given by the arithmetical mean height values $R_a = 0.85$ μm, $R_a = 1.03$ μm and $R_a = 1.53$ μm [microscope images in Fig. 5(a-c)]. The performance of the measurement carried out by the fluorescence vortex topography was assessed in comparison with a commercial 3D profiler (Zygo New View 2000) utilizing coherence scanning interferometry. The 3D surface topography obtained by the vortex localization of fluorescent markers and the commercial 3D profiler is illustrated in Figs. 4(a) and 4(b), respectively. In both measurements made in the area 400×400 μm^2, the same surface with the lowest roughness $R_a = 0.85$ μm was used. The surface topography is determined by a cloud of points providing the surface heights in the transverse measurement positions. The fitting spheres obtained from these points give a radius of $R = 5.03$ mm and $R = 4.99$ mm for the proposed method and the reference measurement, respectively. Although the number of measured points is limited by the number of fluorescent markers adherent to the measured surface [Fig. 4(a)], the obtained radius of the best-fit sphere corresponds well to the value of the reference measurement. Both measured radii are close to the nominal production value $R = 5$ mm.

To evaluate the measurement precision, deviations of the measured heights from the best-fit sphere were determined and illustrated using color scaling for both the vortex topography [Figs. 5(d)–5(f)] and the commercial 3D profiler [Figs. 5(g)–5(i)]. For each measurement, the standard deviation was calculated using data across the whole field of view. When measuring the surface with $R_a = 0.85$ μm, the standard deviation $\sigma = 0.5$ μm was obtained. This value corresponds well to the precision determined in the calibration measurement [Fig. 3(b)]. The best-fit sphere radius $R = 5.62$ mm, determined by the vortex topography for the surface with $R_a = 1.03$ μm [Fig. 5(e)], is larger than the nominal production value, but this deviation is confirmed by the reference measurement giving $R = 5.45$ mm [Fig. 5(h)]. For the surface with $R_a = 1.03$ μm, the commercial profiler seems to have better roughness sensitivity, because the determined standard deviation $\sigma = 1.4$ μm better matches the mean surface roughness than $\sigma = 0.5$ μm obtained in the vortex topography measurement. The advantages provided by the independence of the vortex topography from adverse effects of diffuse light become apparent when measuring the surface with $R_a = 1.53$ μm. Although measurement of surfaces with high curvature and roughness is challenging for proven interferometric methods,

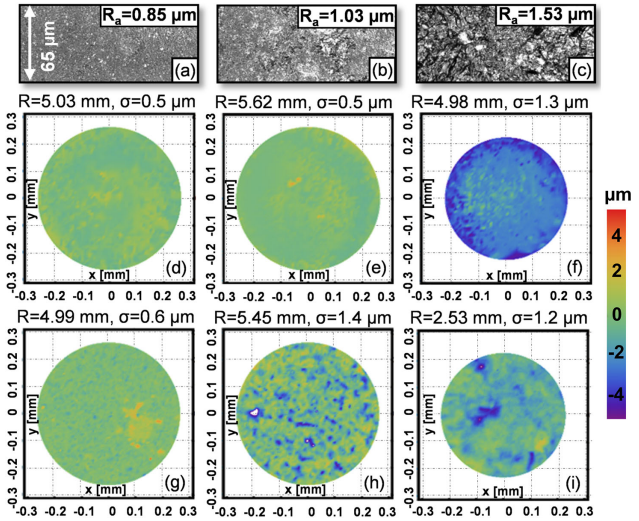

Fig. 5. Comparison of the rough surface measurement using fluorescence vortex topography and commercial 3D profiler. (a)–(c) Microscope images of measured spherical surfaces ($R = 5$ mm) with roughness $R_a = 0.85$ µm, $R_a = 1.03$ µm, and $R_a = 1.53$ µm. (d)–(f) Color-coded map of deviations between the best-fit sphere and the heights of surfaces (a)–(c) measured by vortex topography. (g)–(i) Same as in (d)–(f) but for the measurement using commercial profiler.

the vortex topography was still applicable. The radius of the best-fit sphere $R = 4.98$ mm, close to the nominal production value, was restored with the standard deviation $\sigma = 1.3$ µm corresponding to the mean surface roughness [Fig. 5(f)]. When the commercial profiler was used, large slopes and edges of the surface caused the diffuse light to be deflected outside the optical system, and signal failures made it difficult to process data correctly. In these unfavorable conditions, the radius of the best-fit sphere $R = 2.53$ mm was significantly deviated from the nominal production value [Fig. 5(i)]. Measurements have shown that the fluorescence vortex topography is also useful for determining surface roughness, but appropriate selection of marker sizes is necessary when measuring surfaces of significantly different roughness.

In summary, we have demonstrated a new approach to the topography measurement of rough surfaces. Our method benefits from 3D localization of fluorescent nanospheres adherent to the measured surface. The light used for excitation of the fluorescent markers is bandpass filtered; hence, the measurement is not impaired by diffuse light and the measurement accuracy is maintained even for surfaces with large slopes and roughness. The performed experiments verified the applicability of the method to measuring the surface topography immediately after the rough machining operations, which allows repairing or discarding the optical elements in the phase preceding the time-consuming finishing operations. Thanks to fluorescent marking, the developed technique is also applicable to the measurement of tools used in optical production and a variety of non-optical surfaces only slightly reflecting light.

Funding. Grantová Agentura České Republiky (GA18-01396S); Central European Institute of Technology (LQ1601); H2020 Spreading Excellence and Widening Participation (No. 810626); Univerzita Palackého v Olomouci (IGA PrF 2020 004); Czechoslovak Microscopy Society.

Acknowledgment. We thank company Meopta-optika, s.r.o., for preparing test surfaces and making reference measurements by a commercial profiler. We also thank the Institute of Scientific Instruments of the CAS, v.v.i. (ISI) for imaging rough surfaces on a confocal microscope.

Disclosures. The authors declare no conflicts of interest.

REFERENCES

1. G. Udupa, M. Singaperumal, R. S. Sirohi, and M. P. Kothiyal, Meas. Sci. Technol. **11**, 305 (2000).
2. M. A. Browne, O. Akinyemi, and A. Boyde, Scanning **14**, 145 (1992).
3. C. Zuo, S. Feng, L. Huang, T. Tao, W. Yin, and Q. Chen, Opt. Lasers Eng. **109**, 23 (2018).
4. W. Kapłonek, K. Nadolny, and G. M. Królczyk, Meas. Sci. Rev. **16**, 42 (2016).
5. K. Miura and A. Nose, in *Optical Measurement of Surface Topography* (Springer, 2011), p. 107.
6. P. de Groot, in *Optical Measurement of Surface Topography* (Springer, 2011), p. 167.
7. D. Malacara, ed., *Optical Shop Testing* (Wiley, 2007).
8. T. R. Judge and P. J. Bryanston-Cross, Opt. Lasers Eng. **21**, 199 (1994).
9. K. Hibino, Y. Tani, Y. Bitou, T. Takatsuji, S. Warisawa, and M. Mitsuishi, Appl. Opt. **50**, 962 (2011).
10. B. S. Lee and T. C. Strand, Appl. Opt. **29**, 3784 (1990).
11. A. Harasaki, J. Schmit, and J. C. Wyant, Appl. Opt. **39**, 2107 (2000).
12. G. Häusler, P. Ettl, M. Schenk, G. Bohn, and I. Laszlo, *International Trends in Optics and Photonics*, Springer Series in Optical Sciences (Springer, 1999), Vol. **74**.
13. P. Pavliček and O. Hýbl, Appl. Opt. **47**, 2941 (2008).
14. M. Lee, M. Lew, A. von Diezmann, L. Weiss, Y. Shechtman, and W. E. Moerner, Biophys. J. **110**, 176a (2016).
15. S. Quirin, S. R. P. Pavani, and R. Piestun, Proc. Natl. Acad. Sci. USA **109**, 675 (2012).
16. S. R. P. Pavani, M. A. Thompson, J. S. Biteen, S. J. Lord, N. Liu, R. J. Twieg, R. Piestun, and W. E. Moerner, Proc. Natl. Acad. Sci. USA **106**, 2995 (2009).
17. M. Teich, M. Mattern, J. Sturm, L. Büttner, and J. W. Czarske, Opt. Express **24**, 27371 (2016).
18. P. Bouchal, L. Štrbková, Z. Dostál, and Z. Bouchal, Opt. Express **25**, 21428 (2017).
19. P. Bouchal and Z. Bouchal, J. Opt. **19**, 105606 (2017).